Optical properties of rutile near its fundamental band gap

A. Amtout and R. Leonelli
Département de Physique et Groupe de Recherche en Physique et Technologie des Couches Minces, Université de Montréal, Case Postale 6128, Succursale Centre-Ville, Montréal, Québec, Canada H3C 3J7
(Received 19 September 1994)

We report low-temperature absorption, time-integrated photoluminescence, and resonant-Raman-scattering spectra near the fundamental band gap of TiO_2 single crystals. The photoluminescence spectrum comprises a first peak at $\hbar\omega = 3.031$ eV, followed by several peaks at lower energies. A polarization study of the emission spectrum indicates that the highest energy peak corresponds to $2p_{xy}$ dipole-allowed second-class excitonic transitions while the lower-energy peaks are phonon replicas of the $1s$ quadrupolar exciton. This result is corroborated by time-resolved photoluminescence measurements. The near-band-gap optical response of TiO_2 is thus controlled by two distinct exciton states. The Raman-scattering intensity is found to increase slowly for excitation energies in the range 2.7–3 eV. This indicates that the Raman cross-section enhancement is dominated by virtual transitions involving the first dipole-allowed direct gap at 4.2 eV.

I. INTRODUCTION

Rutile (TiO_2) is a polar material of technological importance since it is used as a substrate in catalytical and electrochemical processes and as a dielectric for integrated electronics.[1,2] It is also of fundamental interest because its high static dielectric constant, strong electron-phonon coupling, and unusual band structure result in near-band-gap optical properties which are still not well understood.

TiO_2 has a tetragonal structure (space group D_{4h}^{14}) which contain six atoms per unit cell.[3] This structure can be seen as a stacking of oxygen octahedra centered on titanium atoms. Band-structure calculations[4,5] indicate that the valence band of rutile is mainly composed of the outermost p electrons from the oxygen atoms, while the lowest conduction band is mostly composed of the excited states of the titanium atoms. The symmetry of these bands is such that a direct band gap with dipole-forbidden transitions at the Γ point is predicted.[4,5] SnO_2 has a band structure similar to that of TiO_2. With a band gap $E_g = 2.31$ eV and an exciton binding energy Ry = 151 meV, it shows exciton lines up to $n = 6$.[6] TiO_2 has an even larger band gap ($E_g > 3$ eV) but, because of its high dielectric constant, the $1s$ exciton binding energy is expected to be less than 10 meV. This makes an exact assignment of the structures seen in the optical spectra difficult. Low-temperature absorption measurements[7,8] have identified a weak absorption peak at $\hbar\omega = 3.031$ eV. It was attributed to a $1s$ electric-quadrupole-allowed excitonic transition. A weaker structure at higher energy was further attributed to the $2p_{xy}$ electric-dipole-allowed excitonic transition. Hyper-Raman-scattering experiments were also performed in the vicinity of the band gap of rutile.[9] These measurements showed an enhancement of the scattering efficiency of the $\Gamma_2'(A_{2u})$ and $\Gamma_5'(E_u)$ phonon modes for $2h\omega = 3.031$ eV. This enhancement was thus associated with the $1s$ exciton state. However, we recently presented preliminary absorption, photoluminescence, and Raman-scattering spectra which cast some doubts on these assignments.[10,11]

In this paper, we present a detailed study of the optical properties of rutile near its fundamental band gap. Time-resolved photoluminescence (TRP), time-integrated photoluminescence (TIP), and resonant-Raman-scattering (RRS) experiments were performed under pulsed excitation conditions on high quality TiO_2 crystals. The observed spectra, which are consistent with the predicted forbidden band gap, indicate that the optical response of TiO_2 is controlled by two distinct exciton states, namely the $1s$ quadrupolar and $2p$ dipolar excitons.

The paper is organized as follows. The experimental setup is described in Sec. II. In the third section, the theoretical background required to analyze the absorption, photoluminescence, and Raman-scattering measurements is developed. The experimental results are presented in Sec. IV, and discussed in Sec. V. Finally, we summarize the results and draw conclusions in Sec. VI.

II. SAMPLES AND EXPERIMENTS

The samples studied in this work are high-purity x-ray-oriented crystals obtained from Commercial Crystal Laboratories. Sample 1, with dimensions $1 \times 1 \times 0.1$ cm^3, has its face oriented along the [001] direction and one of the sides along the [110] direction. Sample 2, with dimensions $1 \times 1 \times 0.2$ cm^3, has its large face oriented along the [100] direction and one of the sides along [001].

The samples were mounted in a helium exchange-gas closed-cycle cryostat which allowed us to vary the temperature between 12 and 300 K. The samples were excited by 2-ns-long pulses generated by a tunable dye laser pumped by a XeCl excimer laser operated at a repetition rate of 20 Hz. For the TRP and TIP measurements, the intensity per pulse and the photon energy were 5 mJ cm^{-2} and 3.26 eV (3800 Å), respectively [using 4,4‴-bis-(2-butyloctyloxy)-p-quarterphenyl (BBQ) as dye]. For the RRS, different dyes were used to cover the range

from 2.7 to 3.12 eV, and the excitation intensity was maintained constant at 1 mJ cm^{-2} per pulse by adjusting the amplification length in the amplifier cell of the dye laser. The emitted and scattered light were focused onto the slits of an I.S.A. HR-320 spectrometer (spectral resolution of 0.5 meV), and detected by a fast multichannel plate photomultiplier tube. The signal was acquired by a Tektronix 7912AD digitizer equipped with a 500-MHz amplifier. The overall time resolution of the system is 1 ns. The time-resolved spectra were obtained by deconvolving the raw data from the system time response with a standard minimization procedure where the photoluminescence dynamics was represented by a linear combination of exponential functions. The TIP spectra were obtained by integrating the digitized signal on a 50-ns-long interval after excitation. Absorption measurements were performed using a white light source and 1-m double spectrometer (spectral resolution of 0.1 meV). The signal was detected with a GaAs photomultiplier tube and acquired with conventional photon-counting techniques.

III. THEORY

A. Luminescence and absorption

The optical transition probability per unit time for a direct recombination (absorption) from an initial state $|\psi_i^n\rangle$ to a final state $|\psi_f^m\rangle$, where n and m are used for the degeneracy of the states, is given by

$$W_{\text{fi}}=\frac{2\pi}{\hbar}\sum_{nm}|\langle\psi_i^n|H_{\text{XR}}|\psi_f^m\rangle|^2\delta(E_f^m-E_i^n)\ , \tag{1}$$

where H_{XR} is the exciton radiation interaction operator. H_{XR} can be developed in terms of electric dipole (ED), electric quadrupole (EQ) and magnetic dipole (MD) components:[12]

$$H_{\text{XR}}=H_{\text{XR}}^{\text{ED}}+H_{\text{XR}}^{\text{EQ}}+H_{\text{XR}}^{\text{MD}}\ , \tag{2}$$

with

$$H_{\text{XR}}^{\text{ED}}=A_0\boldsymbol{\epsilon}_i\cdot\mathbf{p}\ , \tag{3}$$

$$H_{\text{XR}}^{\text{EQ}}=i\frac{A_0}{2}\mathbf{k}\cdot(\mathbf{rp}+\mathbf{pr})\cdot\boldsymbol{\epsilon}_i\ , \tag{4}$$

$$H_{\text{HR}}^{\text{MD}}=i\frac{A_0}{2}(\mathbf{k}\times\boldsymbol{\epsilon}_i)\cdot(\mathbf{r}\times\mathbf{p})\ , \tag{5}$$

where A_0 is the constant amplitude of the external vector potential, $\boldsymbol{\epsilon}_i$ its unit polarization vector, and $\mathbf{k}$ its wave vector. The operator $H_{\text{XR}}^{\text{EQ}}$ can be put in the form

$$\langle\psi_i|\mathbf{rp}+\mathbf{pr}|\psi_r\rangle=im(E_f-E_i)/\hbar\langle\psi_i|\mathbf{rr}|\psi_f\rangle\ . \tag{6}$$

Thus, at resonance,

$$H_{\text{XR}}^{\text{EQ}}=i\frac{A_0}{2}im\omega\mathbf{k}\cdot(\mathbf{rr})\cdot\boldsymbol{\epsilon}_i=i\frac{A_0}{2}(\mathbf{k}\cdot\mathbf{r})(\boldsymbol{\epsilon}_i\cdot\mathbf{r})\ . \tag{7}$$

To find the selection rules, it is useful to put Eq. (7) in the form

$$\begin{aligned}H_{\text{HR}}^{\text{EQ}}\propto{}&\tfrac{1}{2}\epsilon_z k_z(2z^2-x^2-y^2)+\tfrac{1}{2}(\epsilon_x k_x-\epsilon_y k_y)(x^2-y^2)\\&+(\epsilon_y k_z+\epsilon_z k_y)yz+(\epsilon_z k_x+\epsilon_x k_z)xz\\&+(\epsilon_x k_y+\epsilon_y k_x)xy\ ,\end{aligned} \tag{8}$$

where $(2z^2-x^2-y^2)$ belongs to Γ_1, (x^2-y^2) to Γ_3, xy to Γ_4, and xz and yz to Γ_5.

In TiO_2, the symmetries of the valence and conduction bands are Γ_3 and Γ_1 respectively.[4] In the case of Wannier-type excitons, the free exciton wave function can be regarded as a product of an envelope function $F(\mathbf{r}_e-\mathbf{r}_h)$ which describes the relative motion of an electron and a hole, and the Bloch functions $\psi_v^*(\mathbf{r}_h)$ and $\psi_c(\mathbf{r}_e)$ of the valence and conduction states at the critical point considered. The irreducible representation of the envelope functions are Γ_1 for s states, Γ_2' for p_z state and Γ_5' for $p_{x,y}$ states. The exciton state symmetries, given by $\Gamma_c\times\Gamma_v^*\times\Gamma_{\text{env}}$, are therefore Γ_3 for s states, Γ_4' for p_z states, and Γ_5' for $p_{x,y}$ states. Since the electric dipole moment transforms as $\Gamma_2'+\Gamma_5'$ and the magnetic dipole moment as $\Gamma_2+\Gamma_5$, the s excitons can be created only through quadrupolar interaction, and the probability of creation or recombination of $1s$ excitons is given by

$$I_{1s}\propto(\epsilon_x k_x-\epsilon_y k_y)^2\ . \tag{9}$$

We note that $I_{1s}=0$ for $\mathbf{k}\|\mathbf{c}$ or $\boldsymbol{\epsilon}\|\mathbf{c}$. The probabilities of creation or recombination of the $2p_{xy}$ and $2p_z$ excitons are given by

$$I_{2p_{xy}}\propto(\epsilon_x^2+\epsilon_y^2)\ , \tag{10}$$

$$I_{2p_z}=0\ . \tag{11}$$

In absorption, to distinguish between the $1s$ and $2p_{xy}$ excitons, one can choose a configuration where $\mathbf{k}\|\mathbf{c}$, so that in this case $I_{2p_{xy}}\neq0$ and $I_{1s}=0$.

In the case of phonon-assisted transitions, the transition probability per unit time from an exciton with wave vector $\mathbf{K}_X$ to the ground state, involving emission of one photon of wave vector $\mathbf{q}$ and one photon of energy $\hbar\omega$ and wave vector $\mathbf{k}$ through the leading ED interaction is given by[13]

$$W=\frac{2\pi}{\hbar}\sum_{\mathbf{q},\mathbf{K}_X}\sum_{j\mu}\left|\sum_{\beta}\frac{\langle0;n_{\mathbf{K}}|H_{\text{XR}}^{\text{ED}}|\beta,\mathbf{K}_\beta;n_{\mathbf{q}}\rangle\langle\beta,\mathbf{K}_\beta;n_{\mathbf{q}}|H_{\text{XL}}^{(j_i\mu)}|X,\mathbf{K}_X;n_{\mathbf{q}}-1\rangle}{E(\beta,\mathbf{K}_\beta)-\hbar\omega}\right|^2\delta[E(X,\mathbf{K}_X)-\hbar\Omega_{j\mu}(\mathbf{q})-\hbar\omega]\ , \tag{12}$$

where $\hbar\Omega_{j\mu}(\mathbf{q})$ is the energy of the phonon of wave vector $\mathbf{q}$ (μ for the degeneracy) and $|\beta,\mathbf{K}_\beta\rangle$ are exciton intermediate states with wave vector $\mathbf{K}_\beta$. From the conservation of momentum, the left-hand-side matrix element in Eq. (12) is different from zero only if $\mathbf{K}_\beta=\mathbf{k}\approx 0$, and the right-hand-side matrix element then requires $\mathbf{q}=\mathbf{K}_X$. The electronic ground state of the system is completely symmetric, i.e., it belongs to Γ_1. The matrix element $\langle 0|H_{\mathrm{XR}}^{\mathrm{ED}}|\beta,0\rangle$ is therefore different from zero only for $|\beta,0\rangle=|\Gamma_5'\rangle$ and $|\Gamma_2'\rangle$. The allowed phonon symmetries at the center of the Brillouin zone are those contained in the decomposition of $\Gamma_X\times\Gamma_2'$ and $\Gamma_X\times\Gamma_5'$ into the irreducible representations of the point group D_{4h}, where Γ_X is the symmetry of the exciton state $|X,0\rangle$. Thus the phonon replicas of $1s$ excitons are

$$\Gamma_3\times\Gamma_5'=\Gamma_5' ,$$
$$\Gamma_3\times\Gamma_2'=\Gamma_4' . \tag{13}$$

The allowed optical-phonon modes of rutile are[14]

$$\Gamma_{\mathrm{opt}}=\Gamma_1(A_{1g})+\Gamma_2(A_{2g})+\Gamma_3(B_{1g})+\Gamma_4(B_{2y})+\Gamma_5(E_g)+\Gamma_2'(A_{2u})+2\Gamma_3'(B_{1u})+3\Gamma_5'(E_u) . \tag{14}$$

Since there is no phonon of Γ_4' symmetry in rutile, the phonon replicas of the $1s$ exciton are of Γ_5' symmetry. The phonon replicas of $2p_{xy}$ excitons are

$$\Gamma_2'\times\Gamma_5'=\Gamma_5 ,$$
$$\Gamma_5'\times\Gamma_5'=\Gamma_1+\Gamma_2+\Gamma_3+\Gamma_4 , \tag{15}$$

and those of the p_z excitons are

$$\Gamma_2'\times\Gamma_4'=\Gamma_3 ,$$
$$\Gamma_5'\times\Gamma_4'=\Gamma_5 . \tag{16}$$

Of all the allowed phonon replicas, only the phonons of Γ_5' symmetry are polar. Thus the coupling constants between the excitons and the three longitudinal-optical (LO) phonons of Γ_5' symmetry are much larger than the allowed nonpolar phonon vibrations. At low temperature, and in thermal equilibrium, the exciton population is concentrated around $\mathbf{K}=\mathbf{K}_X\approx 0$. In the limit $\mathbf{K}=\mathbf{K}_X=0$, the polarization properties of the phonon replicas of Γ_5' symmetry are given by

$$I_{1s-\mathrm{LO}(\Gamma_5')}\propto(\epsilon_x^2+\epsilon_y^2) . \tag{17}$$

TABLE I. Irreducible representations (I.R.) of H_{X-R} and polarization dependence of $1s$, $1s$-LO, $2p$, and $2p$-LO emission intensities for ED, MD, and EQ interactions.

	ED	MD	EQ
I.R.	$\Gamma_2'+\Gamma_5'$	$\Gamma_2+\Gamma_5$	$\Gamma_1+\Gamma_3+\Gamma_4+\Gamma_5$
I_{1s}	0	0	$(\epsilon_x k_x-\epsilon_y k_y)^2$
$I_{1s\text{-LO}}$	$\epsilon_x^2+\epsilon_y^2$	~ 0	~ 0
$I_{2p_{x,y}}$	$\epsilon_x^2+\epsilon_y^2$	0	0
I_{2p_z}	0	0	0
$I_{2p\text{-LO}}$	~ 0	~ 0	~ 0

We note that the polarization properties of the $2p_{xy}$ excitons and the phonon replicas of the $1s$ quadrupolar excitons are the same. All these results are summarized in Table I.

When one includes the spin-orbit interaction, the symmetries of the valence and conduction bands are Γ_6 and Γ_7 respectively.[5] The symmetry of the $1s$ exciton is

$$\Gamma_1\times\Gamma_6\times\Gamma_7=\Gamma_3+\Gamma_4+\Gamma_5 , \tag{18}$$

that of the $2p_{xy}$ exciton

$$\Gamma_5'\times\Gamma_6\times\Gamma_7=\Gamma_1'+\Gamma_2'+\Gamma_3'+\Gamma_4'+2\Gamma_5' , \tag{19}$$

and that of the p_z exciton

$$\Gamma_2'\times\Gamma_6\times\Gamma_7=\Gamma_3'+\Gamma_4'+\Gamma_5' . \tag{20}$$

From the symmetries of the ED, EQ, and MD (summarized in Table I), we find that the $1s$ and $2p$ excitons are allowed in both polarization configurations ($\mathbf{E}\|\mathbf{c}$ and $\mathbf{E}\perp\mathbf{c}$) through the EQ and ED (second class) interaction, respectively. By including the spin-orbit interaction in the band-structure calculation, the symmetry of the $1s$ exciton passes from Γ_3 to $\Gamma_3+\Gamma_4+\Gamma_5$. However, if the spin-orbit interaction is small, then the wave functions of Γ_4 and Γ_5 symmetries will correspond to small corrections of the wave function of Γ_3 symmetry. The optical matrix elements corresponding to the transition Γ_4 to Γ_1 and Γ_5 to Γ_1 (Γ_1 is the symmetry of the fundamental state) will thus be small compared to that of the transition Γ_3 to Γ_1. Similar conclusions can be reached in the case of the $2p_{xy}$ exciton.

B. Resonant Raman scattering

The intensity of the first-order Raman scattering near resonance with an exciton is given by[15,16]

$$I(\omega_1,\omega_s,\Omega)\propto\left|\sum_{a,b}\frac{\langle f|H_{\mathrm{XR}}^{(2)}|a\rangle\langle a|H_{\mathrm{XL}}|b\rangle\langle B|H_{\mathrm{XR}}^{(1)}|i\rangle}{(\omega_s-\omega_a)(\omega_1-\omega_b)}+C\right|^2\delta(\omega_1-\omega_s-\Omega) , \tag{21}$$

where ω_1 and ω_s are the frequencies of the incident and scattered radiation, respectively; Ω is the phonon frequency; $|i\rangle$, $|f\rangle$, and $|a\rangle$ and $|b\rangle$ are initial, final, and intermediate states; $\hbar\omega_a$ and $\hbar\omega_b$ are complex intermediate state energies; and H_{XR} and H_{XL} are the exciton-radiation and exciton-lattice interactions.

Away from any excitonic resonances, the Raman-active phonon modes are those contained in the decom-

position of the tensor **rr** into the irreducible representation of the point group D_{4h}, which are

$$\begin{aligned}&\Gamma(y^2)=\Gamma(x^2)=\Gamma_1+\Gamma_3\ ,\\&\Gamma(z^2)=\Gamma_1\ ,\\&\Gamma(xy)=\Gamma_4\ ,\\&\Gamma(xz)=\Gamma(yz)=\Gamma_5\ ,\end{aligned}\tag{22}$$

and, as shown by Loudon,[15] when Ω is small compared to $\omega_\alpha-\omega_1$ and $\omega_\alpha-\omega_s$ ($\alpha=a$ and b), the Raman tensor is symmetrical in the photon polarization. The situation is different near resonance. Symmetry breaking for intrinsic Raman scattering can occur when the matrix element of H_{XR}^{ED} between the initial state $|i\rangle$ and the resonant state $|b\rangle=|X\rangle$ is zero. In this case $H_{XR}^{(1)}$ should be replaced by H_{XR}^{EQ} and (or) H_{XR}^{MD} and $H_{XR}^{(2)}$ can be taken as H_{XR}^{ED}. The operator H_{XR}^{EQ} transforms as a second rank tensor **rr** and H_{XR}^{ED} transforms as **r**. In TiO_2, the Raman-active modes are therefore those contained in the decomposition of the components of the third rank tensor **rrr** into the irreducible representations of D_{4h}, which are

$$\Gamma_{\text{ED-EQ}}=\Gamma_2'+\Gamma_3'+\Gamma_5'\ .\tag{23}$$

When $H_{XR}^{(1)}$ is taken as H_{XR}^{MD}, which transforms as an axial vector, the Raman-active modes of the ED-MD diffusion process are

$$\Gamma_{\text{ED-MD}}=\Gamma_2'+\Gamma_3'+\Gamma_5'\ .\tag{24}$$

In TiO_2, we are concerned with excitons of Γ_3 symmetry for the $1s$ exciton and Γ_5' symmetry for the $2p_{xy}$. Thus, at resonance with the $1s$ exciton, the symmetry of the active Raman phonon modes are

$$\begin{aligned}&\Gamma_3\times\Gamma_5'=\Gamma_5'\ ,\\&\Gamma_3\times\Gamma_2'=\Gamma_4'\ .\end{aligned}\tag{25}$$

As mentioned in Sec. III A, there is no phonon mode of Γ_4' symmetry in TiO_2. Therefore, at resonance with the $1s$ exciton, only $\Gamma_5'(E_u)$ Raman modes are allowed by the selection rules. Since these modes are polar, their longitudinal components carry a macroscopic electric field **E** which causes a shift of the LO-phonon energies, resulting in LO-TO splitting.

At resonance with the $2p_{xy}$ exciton, the operators $H_{XR}^{(1)}$ and $H_{XR}^{(2)}$ are taken as H_{XR}^{ED}. Since $H_{XR}^{(1)}$ can be taken to transform as x or y but not as z, and $H_{XR}^{(2)}$ transforms as **r**, the Raman-active phonon modes are those contained in the decomposition of the components (x^2,y^2,xy,xz,yz) into the irreducible representations of the point group D_{4h} which are $\Gamma_1(A_{1g})$, $\Gamma_3(B_{1g})$, $\Gamma_4(B_{2g})$, and $\Gamma_5(E_g)$. The above results are summarized in Table II.

TABLE II. Multipole-dipole Raman-scattering selection rules at resonance and away from resonance.

$H_{XR}^{(1)}$	$H_{XR}^{(2)}$	Resonance	Transforms as	Raman-active modes
EQ	ED	No	(**r**)(**rr**)	$\Gamma_2'+\Gamma_3'+\Gamma_5'$
MD	ED	No	(**r**)(**r**×**p**)	$\Gamma_2'+\Gamma_3'+\Gamma_5'$
EQ	ED	$1s$ exciton	$(\mathbf{r})(x^2-y^2)$	Γ_5'
ED	ED	$2p_{xy}$ exciton	$(\mathbf{r})(x,y,0)$	$\Gamma_1+\Gamma_3+\Gamma_4+\Gamma_5$

At resonance with the $2p_{xy}$ excitons, the Raman-scattering intensity is composed of two contributions: those of second-class excitons (labeled r) and those which come essentially from the valence bands of symmetries Γ_2' and Γ_5' located at approximately -4 eV from the conduction band of symmetry Γ_1 (labeled nr).[17] At resonance, the Γ_1 and Γ_5 Raman tensors are given by

$$T(\Gamma_1)=\begin{bmatrix}T_{xx}&0&0\\0&T_{xx}&0\\0&0&0\end{bmatrix}_r+\begin{bmatrix}T_{xx}&0&0\\0&T_{xx}&0\\0&0&T_{zz}\end{bmatrix}_{nr},\tag{26}$$

$$T(\Gamma_5,1)=\begin{bmatrix}0&0&T_{zx}\\0&0&0\\0&0&0\end{bmatrix}_r+\begin{bmatrix}0&0&T_{zx}\\0&0&0\\T_{xz}&0&0\end{bmatrix}_{nr},\tag{27}$$

$$T(\Gamma_5,2)=\begin{bmatrix}0&0&0\\0&0&T_{zy}\\0&0&0\end{bmatrix}_r+\begin{bmatrix}0&0&0\\0&0&T_{zy}\\0&T_{yz}&0\end{bmatrix}_{nr},\tag{28}$$

and the scattering intensity is proportional to

$$\begin{aligned}&I(\Gamma_1)\propto|\epsilon_i\cdot T(\Gamma_1)\cdot\epsilon_s|^2\ ,\\&I(\Gamma_5)\propto\sum_{j=1}^{2}|\epsilon_i\cdot T(\Gamma_5,j)\cdot\epsilon_s|^2\ .\end{aligned}\tag{29}$$

Let $|s,\lambda\rangle$ denote the exciton states of Γ_2' and Γ_5' symmetries having s-type envelope-function symmetries and formed by pairs of valence and conduction bands (Γ_2',Γ_1) and (Γ_5',Γ_1), respectively, and $|p_{x,y},\eta;\Gamma_5'\rangle$ the states of excitons having p-type envelope functions formed by the valence and conduction bands (Γ_3,Γ_1). The components of the tensors can be deduced from the following equations:

$$\begin{aligned}A_r=&\sum_{\eta,\eta'}\frac{\langle\Gamma_1|H_{XR}^{(ED)}|p_{x,y},\eta\rangle\langle p_{x,y},\eta|H_{XL}^{(j,\nu)}|p_{x,y},\eta'\rangle\langle p_{x,y},\eta'|H_{XR}^{(ED)}|\Gamma_1\rangle}{(E_\eta+i\Gamma_\eta-\hbar\omega_s)(E_{\eta'}+i\Gamma_{\eta'}-\hbar\omega_i)}\\&+\sum_{\lambda,\eta'}\frac{\langle\Gamma_1|H_{XR}^{(ED)}|s,\lambda\rangle\langle s,\lambda|H_{XL}^{(j,\nu)}|p_{x,y},\eta'\rangle\langle p_{x,y},\eta'|H_{XR}^{(ED)}|\Gamma_1\rangle}{(E_\lambda+i\Gamma_\lambda-\hbar\omega_s)(E_{\eta'}+i\Gamma_{\eta'}-\hbar\omega_i)}\end{aligned}\tag{30}$$

and

$$A_{nr}=\sum_{\lambda\lambda'}\frac{\langle\Gamma_1|H_{\rm XR}^{(\rm ED)}|s,\lambda\rangle\langle s,\lambda|H_{\rm HL}^{(j,\nu)}|s,\lambda'\rangle\langle s,\lambda'|H_{\rm XR}^{(\rm ED)}|\Gamma_1\rangle}{(E_\lambda+i\Gamma_\lambda-\hbar\omega_s)(E_{\lambda'}+i\Gamma_{\lambda'}-\hbar\omega_i)}+A(\omega)\ , \tag{31}$$

where $A(\omega)$ is the contribution from five other terms.

IV. RESULTS

Figure 1 shows an absorption spectrum obtained in the configuration where $\mathbf{k}\|\mathbf{c}$ at $T=6$ K. The peak at 3.031 eV is only present for $\mathbf{E}\perp\mathbf{c}$. The selection rules given in Table I allow us to associate this peak with the $2p_{xy}$ exciton.

Figure 2 shows TIP spectra at $T=12$ K. The energy position of peaks $A-F$ are, respectively, 3.031, 2.989, 2.977, 2.934, 2.839, and 2.737 eV. Peaks $B-F$ are shifted with respect to peak A by 42, 54, 97, 192 (2×96), and 294 meV (3×98), respectively. These energy shifts are close to the energy of the longitudinal-optical phonons of Γ_5' symmetry measured by infrared absorption and neutron scattering,[3,18] which are 46, 57, and 100 meV. It thus appears that peaks $B-F$ are phonon replicas of Γ_5' symmetry of the $1s$ exciton, since $2p_{xy}$ excitons do not couple to polar phonons of Γ_5' symmetry (see Sec. III).

Polarization and lifetime measurements were performed to further identify the origin of peak A. The polarization dependence of the luminescence is related to the theoretical expressions developed in Sec. III A by

$$I_{\rm ex}=I_0\int_0^{2\pi}I_{\rm th}\cos^2\gamma\,d\gamma\ , \tag{32}$$

where γ is the angle between the polarizer axis and the electric field of the electromagnetic wave [$\gamma=\beta-\alpha$; see Fig. 3(a)]. The components of the wave vector and the electric field of the electromagnetic waves are

$$\begin{aligned}&\mathbf{k}=k_0(\sin\theta\cos\phi,\sin\theta\sin\phi,\cos\theta)\ ,\\&\boldsymbol{\epsilon}=\epsilon_0(\cos\alpha\boldsymbol{\epsilon}_s+\sin\alpha\boldsymbol{\epsilon}_p)\ ,\end{aligned} \tag{33}$$

with

$$\begin{aligned}&\boldsymbol{\epsilon}_p=(-\cos\theta\cos\phi,-\cos\theta\sin\phi,\sin\theta)\ ,\\&\boldsymbol{\epsilon}_s=(\sin\phi,-\cos\phi,0)\ ,\end{aligned} \tag{34}$$

and $\boldsymbol{\epsilon}_s\perp\boldsymbol{\epsilon}_p\perp\mathbf{k}$. The measured intensities for $1s$ excitons are therefore

$$I_{1s}=I_0[A(1+2\cos^2\beta)+B(1+2\sin^2\beta)-2C\sin2\beta]\ , \tag{35}$$

where β is the angle between the polarizer axis and $\boldsymbol{\epsilon}_s$ [see Fig. 3(b)], and

$$\begin{aligned}&A=\sin^2\theta\sin^2\phi\ ,\\&B=\sin^2\theta\cos^2\phi\cos^2\theta\ ,\\&C=\tfrac{1}{2}\sin4\phi\cos\theta\sin^2\theta\ .\end{aligned} \tag{36}$$

For $2p_{xy}$ excitons and phonon replicas of $1s$ excitons, the luminescence is given by

$$\begin{aligned}I_{2p_{xy}}=I_{1s\text{-LO}}=I_0[&(3+\cos^2\theta)\cos^2\beta\\&+(1+3\cos^2\theta)\sin^2\beta]\ .\end{aligned} \tag{37}$$

We have investigated the polarization dependence of the emission intensities of peaks A and D for two different configurations: (a) for the wave vector of the light $\mathbf{k}\|[001]$, and (b) $\mathbf{k}\|[1\bar{1}0]$. From Eqs. (35) and (37), one finds

$$I_{2p_{xy}}^{(a)}\propto I_{1s\text{-LO}}^{(a)}=\text{const}\ , \tag{38}$$

$$I_{1s}^{(a)}=0\ , \tag{39}$$

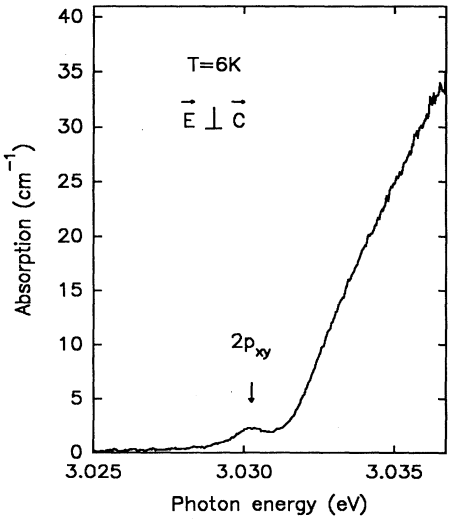

FIG. 1. Absorption spectrum of sample 1 obtained in the configuration where $\mathbf{k}\|\mathbf{c}$.

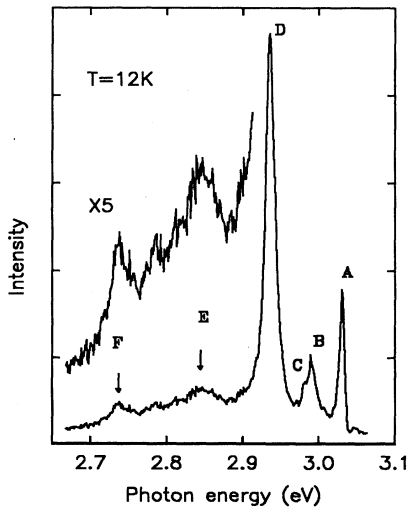

FIG. 2. Time-integrated PL spectra of TiO_2 at $T=12$ K obtained with the excitation energy tuned at 3.26 eV.

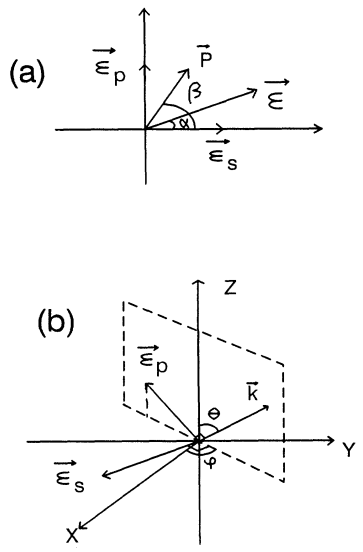

FIG. 3. (a) Orientation of the polarizer axis with respect to the electric vector ϵ of the electromagnetic (EM) radiation and the unit vector ϵ_s (or ϵ_p). (b) Orientation of the unit vectors ϵ_s and ϵ_p, and the wave vector $\mathbf{k}$ of the EM radiation with respect to the crystallographic axes (XYZ).

$$I_{1s}^{(b)} \propto I_{2p_{xy}}^{(b)} \propto I_{1s\text{-LO}}^{(b)} \propto (1+2\cos^2\beta) , \tag{40}$$

where $I^{(a)}$ and $I^{(b)}$ are the emission intensities for the (a) and (b) configurations, and β is the angle between the polarizer axis and the [110] direction ($\epsilon_s \| [110]$).

Figure 4 shows the polarization dependence of the emission intensity of peaks A and D in configuration (a). As can be seen, the intensity is approximately constant. The fluctuations of about 15% from the mean value can be attributed to a depolarization effect caused by surface rugosities, and to the 7° angle over which the signal is collected. Figure 5 shows the signal obtained in configuration (b). The solid line corresponds to the expression given by Eq. (40). These curves indicate clearly that peak A corresponds to the recombination of $2p_{xy}$ excitons, and that peak D is a one-phonon replica of $1s$ quadrupolar excitons.

Figure 6 shows the TRP for peaks A and D. The experimental data are well reproduced by convoluting the system time response with a single-exponential function. We find lifetimes of 1.8 and 3.1 ns for peaks A and D, respectively. The lifetime of $2p_{xy}$ excitons is expected to be shorter than that of 1-s excitons. Furthermore, the life-

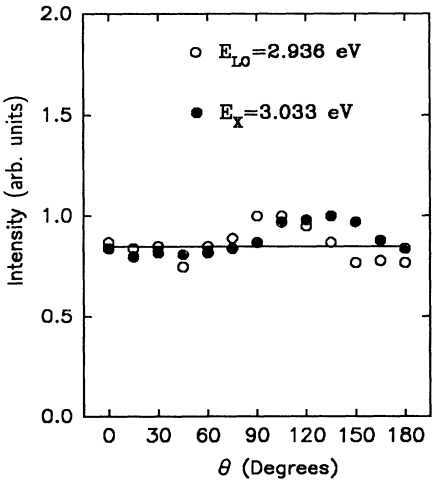

FIG. 4. Polarization dependence of the emission intensity of peaks A and D in configuration (a).

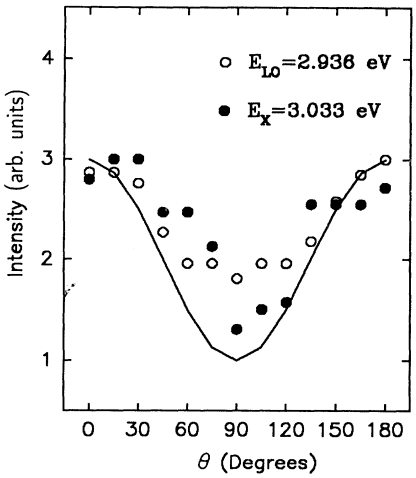

FIG. 5. Polarization dependence of the emission intensity of peaks A and D in configuration (b).

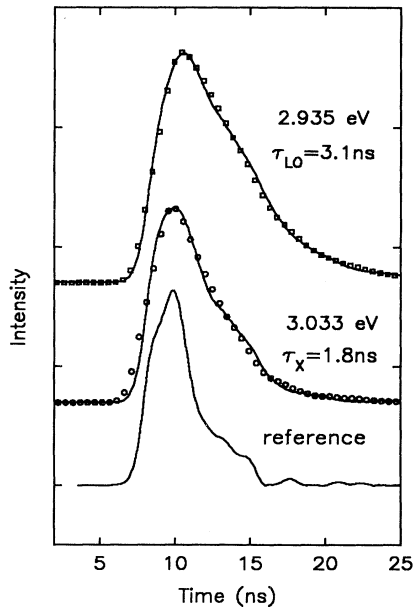

FIG. 6. Emission intensity as a function of time for peaks A and D. Open circles: experimental data. Solid line: best fit using a single-exponential model.

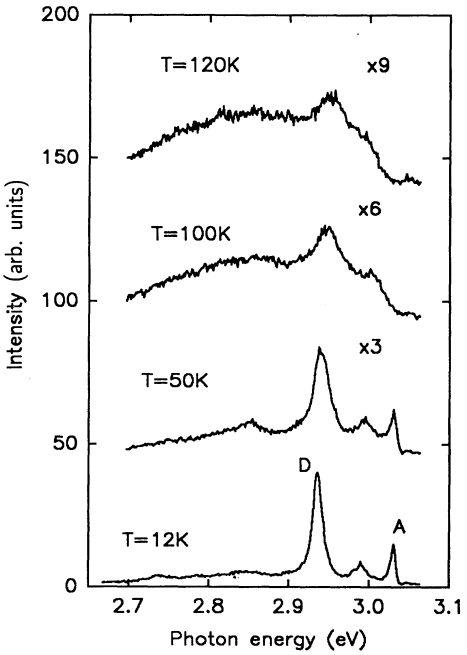

FIG. 7. Time-integrated PL spectra as a function of temperature with an excitation energy $\hbar\omega = 3.26$ eV.

time of phonon replicas should be the same as that of the exciton population involved. The measurements shown in Fig. 6 therefore corroborate our attribution of peak A to a direct $2p_{xy}$ exciton recombination and peak D to a phonon replica of $1s$ dipole-forbidden excitons. Figure 7 shows the temperature evolution of the time-integrated PL. Peak A disappears above 70 K and does not show any energy shift as a function of temperature. For the phonon replicas, we observe a shift approximately equal to the expected shift $k_B \Delta T$.[19,20] Here again, the temperature dependence of the PL intensity supports our attribution of peaks A and $B-F$ to distinct exciton populations.

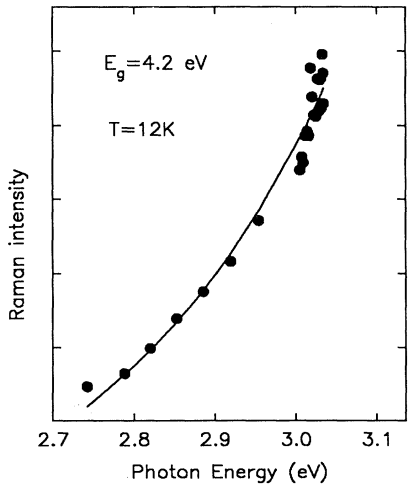

FIG. 9. Resonance curve of the Γ_1 Raman mode in sample 1. The points are the experimental data, and the solid line represents the fit using Eq. (41).

Figure 8 shows the Raman spectrum obtained with the energy of the incident photon tuned at 3.031 eV in the $z(x',\sigma)y'$ configuration ($x'=[110]$, $y'=[\bar{1}10]$, and σ is unpolarized). The energy shift with respect to the laser line of the two peaks are 56 and 76 meV. These energies correspond to the $\Gamma_5(E_g)$ and $\Gamma_1(A_{1g})$ phonon modes, respectively.[21] Figure 9 shows the Raman-scattering intensity of the Γ_1 peak as a function of excitation energy at $T=12$ K. The solid curve represents a parametrized expression deduced from Eqs. (30) and (31):

$$I = I_0 \left[c + \frac{b}{(E_g - \hbar\omega_i - 0.076)(E_g - \hbar\omega_i)} \right]^2 , \qquad (41)$$

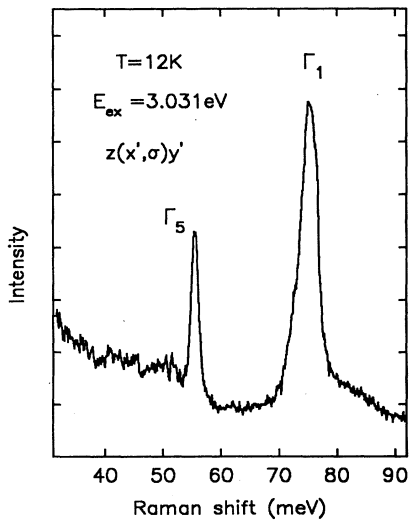

FIG. 8. Raman spectrum from sample 1 with the excitation energy tuned at 3.031 eV.

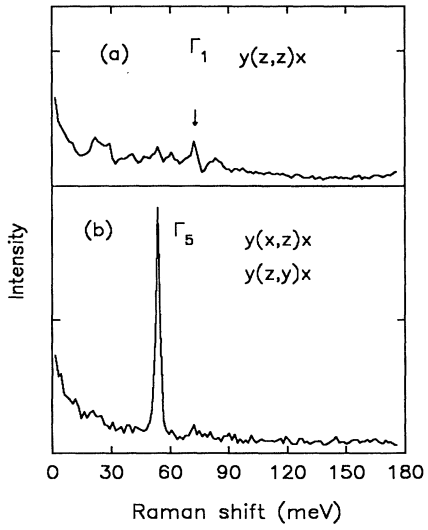

FIG. 10. Raman and PL spectra from sample 1 obtained with the excitation energy tuned at (a) 3065 and (b) 3044 meV.

with $E_g=4.2$ eV, $c=0.4$, and $b=3.2$. These results are at variance with a previously published resonant Raman curve.[11] The discrepancy comes from the fact that our earlier results were not corrected to take into account the onset of absorption in our samples for $\hbar\omega > 3.033$ eV. Given the geometry of our measurements, the data shown in Fig. 9 were corrected using the following expression:

$$I(\hbar\omega)=I_m(\hbar\omega)\frac{\alpha(\hbar\omega)d}{\{1-\exp[-\alpha(\hbar\omega)d]\}} , \quad (42)$$

where $I_m(\hbar\omega)$ corresponds to the measured signal, $\alpha(\hbar\omega)$ is the absorption coefficient, and d is the sample thickness. Figure 10 shows the Raman spectra obtained when the energy of the incident photon is tuned at 3.031 eV in the $y(z,z)x$ configuration for the upper spectrum, and in $y(x,z)x$ and $y(z,y)x$ for the lower spectrum. The intensity of the Γ_5 mode in both configurations is the same, indicating that the Γ_5 tensor is symmetrical to the interchange of the unit polarization vector of the incident and scattered light ϵ_i and ϵ_s, and thus that the contribution from resonantly excited $2p_{xy}$ excitons is much smaller than the nonresonant contributions.

Figure 11 shows spectra composed of Raman and luminescence peaks obtained with the laser line tuned just above the $2p_{xy}$ exciton peak ($\hbar\omega=3.044$ and 3.065 eV). Peaks labeled Γ_5 and Γ_1 are Raman modes, identified by their shift with respect to the energy of the laser line, while peak A has been assigned to the $2p_{xy}$ exciton emission and peaks $B-D$ to the phonon replicas of the $1s$ quadrupolar exciton. A similar coexistence of Raman and luminescence lines is also found in Cu_2O obtained when the laser energy is tuned just above the 1-s quadrupolar exciton.[22] Figure 12 shows the photoluminescence excitation (PLE) spectra of the phonon replica of energy 100 meV (peak D) at $T=12$ K. There is a clear onset of the emission intensity at $\hbar\omega=3.045$ eV, but no resonance with exciton states can be observed.

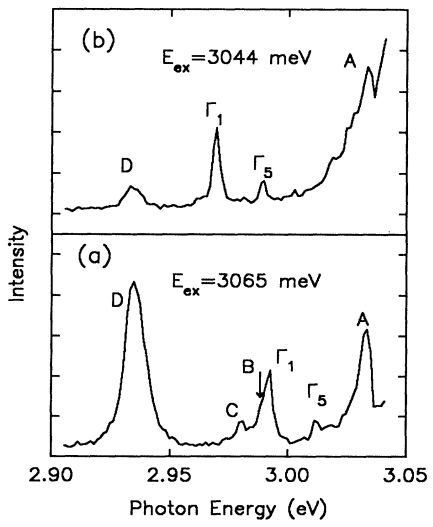

FIG. 11. Raman spectra from sample 2; (a) $y(z,z)x$ configuration; (b) $y(x,z)x$ and $y(z,y)x$ configurations.

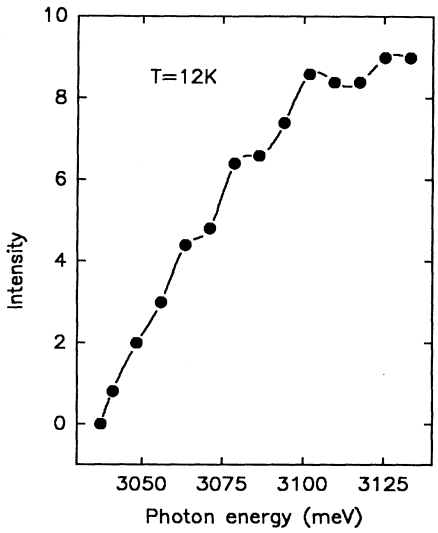

FIG 12. Photoluminescence excitation (PLE) spectra of the phonon replica of energy 100 meV (peak D) obtained at $T=12$ K.

V. DISCUSSION

The absorption, polarized TIP, and TRP spectra are all consistent with the attribution of the 3.031-eV absorption and luminescence peaks to the $2p_{xy}$ exciton state. However, the excitation wavelength dependence of the Raman signal is well represented by Eq. (41). This indicates that the Raman signal enhancement corresponds to a nonresonant process which involves s-symmetry exciton states formed by the Γ_1 conduction band and Γ_5' and (or) Γ_2' valence bands located at around 4 eV below in energy. In order to understand this result, we note that, according to the reflectivity measurements of Cardona and Harbeke[17] at $T=300$ K, the refractive and absorption indices for E⊥c are $n=4$ and $k=2$ for photon energies $\hbar\omega=4$ eV. The corresponding absorption coefficient is

$$\alpha=\frac{2k\omega}{c}\approx 8\times 10^5 \text{ cm}^{-1} . \quad (43)$$

The transition matrix element is given by

$$|M|^2\approx Cnm^2\omega\alpha . \quad (44)$$

Equations (30) and (31) can be written as

$$A_r(1)=\frac{|M_{2p}|^2|\langle p_{xy},\eta|H_{\rm XL}|p_{xy},\eta\rangle|}{|(E_{2p}-\hbar\omega_s)(E_{2p}-\hbar\omega_i+i\Gamma)|} , \quad (45)$$

$$A_r(2)=\frac{|M_{1s}M_{2p}||\langle 1s,\lambda|H_{\rm XL}|p_{xy},\eta\rangle|}{|(E_{1s}-\hbar\omega_s)(E_{2p}-\hbar\omega_i+i\Gamma)|} \quad (46)$$

and

$$A_{nr}=\frac{|M_{1s}|^2|\langle 1s,\lambda|H_{\rm XL}|1s,\lambda\rangle|}{(E_{1s}-\hbar\omega_s)^2} , \quad (47)$$

with $|M_{1s}|^2=Cn_1m^2\hbar\omega_1\alpha_1$ and $|M_{2p}|^2=Cn_2m^2\omega_2\alpha_2$, where $\hbar\omega_1=4$ eV, $\alpha_1=8\times 10^5$ cm^{-1}, $n_1=4$, $\hbar\omega_2=3$ eV,

$\alpha_2=4\ \mathrm{cm}^{-1}$, $n_2=3$, and $\Gamma\approx 4$ meV. Thus

$$\left|\frac{A_r(1)}{A_{\mathrm{nr}}}\right|\approx\frac{1}{75}\left|\frac{\langle p_{xy},\eta|H_{\mathrm{XL}}|p_{xy},\eta\rangle}{\langle 1s,\lambda|H_{\mathrm{XL}}|1s,\lambda\rangle}\right| . \tag{48}$$

Assuming $|\langle p_{xy},\eta|H_{\mathrm{XL}}|p_{xy},\eta\rangle|\approx|\langle 1s,\lambda|H_{\mathrm{XL}}|1s,\lambda\rangle|$, one obtains $|A_r(1)|\ll|A_{\mathrm{nr}}|$. On the other hand,

$$\left|\frac{A_r(2)}{A_{\mathrm{nr}}}\right|\approx\left|\frac{\langle 1s,\lambda|H_{\mathrm{XL}}|p_{xy},\eta\rangle}{\langle 1s,\lambda|H_{\mathrm{XL}}|1s,\lambda\rangle}\right| . \tag{49}$$

Since $\langle 1s,\lambda|H_{\mathrm{XL}}|2p_{xy},\eta\rangle\ll\langle 1s,\lambda|H_{\mathrm{XL}}|1s\lambda\rangle$, $|A_r(2)/A_{\mathrm{nr}}|\ll 1$, and we conclude that $|A_r|\ll|A_{\mathrm{nr}}|$. This analysis probably explains the absence of any enhancement of the Raman-scattering cross section near the $2p_{xy}$ exciton.

Watanabe and co-workers[9] performed resonant hyper-Raman scattering near the fundamental band gap of TiO_2. They found a peak at 3.031 eV in the configurations $x'(y'y',\sigma)z$ and $y(xx,x+z)\bar{y}$, where x', y', and σ are the [110] and [1$\bar{1}$0] directions and unpolarized radiation, respectively, which they associated with the $1s$ quadrupolar exciton. However, neglecting the spin-orbit coupling, it can be shown[23] that the two-photon polarization dependence of the $1s$ quadrupolar exciton is given by

$$M_{1s}=\sum_j\frac{\langle 1s,\Gamma_3|H_{\mathrm{XR}}^{(\mathrm{ED})}|j\rangle\langle j|H_{\mathrm{XR}}^{(\mathrm{ED})}|\Gamma_1\rangle}{E_j-\hbar\omega_i}$$
$$=c(\epsilon_x^2-\epsilon_y^2) , \tag{50}$$

where c is a constant and $\hbar\omega_i$ is the energy of the incident photon. From this equation, we conclude that the probability of creation of a $1s$ exciton by two-photon absorption in the $x'(y'y',\sigma)z$ configuration is zero. In the configuration $y(xx,x+z)\bar{y}$, the intraband Fröhlich exciton-phonon interaction matrix element between the $2p_x$ exciton of Γ_5' symmetry (not $2p_y$) and $1s$ exciton of Γ_3 is zero, i.e., $\langle p_x;\Gamma_5'|H_{\mathrm{XL}}^F|1s;\Gamma_3\rangle=0$. We propose that the hyper-Raman peak at 3.031 eV corresponds to the $2p_{xy}$ exciton as in absorption and photoluminescence experiments. In this case the amplitude of the resonant hyper-Raman-scattering is given by

$$A_m=\sum_{i,j}\frac{\langle\Gamma_1|H_{\mathrm{XR}}|i\rangle\langle i|H_{\mathrm{XL}}^F|2p_{xy}\rangle\langle 2p_{xy}|H_{\mathrm{XR}}|j\rangle\langle j|H_{\mathrm{X\Gamma}}|\Gamma_1\rangle}{(\hbar\omega-E_i-\hbar\Omega)(2\hbar\omega-E_{2p_{xy}})(\hbar\omega-E_j)}+C , \tag{51}$$

where the summation i is over all the states $|i\rangle=|is,\Gamma_5'\rangle$ and $|ip_{xy},\Gamma_5'\rangle$, $i=1,2\ldots$ for the s states and $i=2,3,\ldots$ for the p states.

VI. CONCLUSION

We have presented a detailed study of the optical properties of rutile near its fundamental band gap. Absorption spectra reveal a peak at 3.031 eV in a configuration where $\mathbf{E}\perp\mathbf{c}$ and $\mathbf{k}\|\mathbf{c}$. The selection rules inferred from band-structure calculations indicate that this peak cannot correspond to an optical transition involving the $1s$ quadrupolar exciton state. TIP spectra reveal a luminescence peak at $\hbar\omega=3.031$ eV, followed by several peaks at lower energies which are separated from the first one by energies close to those of Γ_5' symmetry optical phonons. A study of the polarization dependence of the emission peaks allow us to attribute the peak at 3.031 eV to $2p_{xy}$ excitons, and the peaks at lower photon energies to phonon replica of $1s$ quadrupolar excitons. From TRP measurements, we find lifetimes of 1.8 and 3.1 ns for the $2p_{xy}$ exciton recombination and the phonon replicas, respectively. These results indicate that the near-band-gap optical response of TiO_2 is controlled by two distinct exciton states: shorter-lived $2p_{xy}$ excitons give rise to the absorption and emission peaks through dipole-allowed second-class optical transitions, while longer-lived $1s$ quadrupolar excitons are seen in luminescence through phonon-assisted emission.

We also find that the Raman-scattering intensity varies slowly in the range 2.7–3 eV. The experimental data are well reproduced by a model which involves $1s$ excitons formed by the conduction band and lower-energy valence bands. We deduce that there is a direct allowed gap at 4.2 eV, a value close to that found previously by reflectivity measurements. We explain the absence of any enhancement of the Raman intensity near the fundamental gap of TiO_2 by the fact that the resonant contributions to the Raman cross section remain much smaller that the nonresonant ones.

ACKNOWLEDGMENTS

This research was supported by the Natural Sciences and Engineering Research Council of Canada (NSERC), and by the Fonds pour la Formation de Chercheurs et l'Aide à la Recherche (FCAR Québec).

[1]K. M. Glassford, N. Troullier, J. L. Martins, and J. R. Chelikowsky, Solid State Commun. **76**, 635 (1990).
[2]K. M. Glassford and J. R. Chelikowsky, Phys. Rev. B **45**, 3874 (1992).
[3]J. G. Traylor, H. G. Smith, R. M. Nicklow, and M. K. Wilkinson, Phys. Rev. B **3**, 3457 (1971).
[4]N. Daude, C. Gout, and C. Jonanin, Phys. Rev. B **15**, 5292 (1977).

[5]J. L. Jourdan, C. Gout, and J. P. Albert, Solid State Commun. **31**, 1023 (1979).
[6]For a review of the optical properties of direct forbidden band-gap materials, see V. T. Agekyan, Phys. Status Solidi A **43**, 11 (1977).
[7]J. Pascual, J. Camassel, and H. Mathiew, Phys. Rev. B **18**, 5606 (1978).
[8]J. Pascual, J. Camassel, and H. Mathiew, Phys. Rev. Lett. **39**, 1490 (1977).
[9]K. Watanabe and K. Inoue, Phys. Rev. B **41**, 957 (1990); K. Watanabe, K. Inoue, and F. Minami, *ibid.* **46**, 2024 (1992).
[10]A. Amtout and R. Leonelli, Solid State Commun. **84**, 349 (1992).
[11]A. Amtout and R. Leonelli, Phys. Rev. B **46**, 15 550 (1992).
[12]J. L. Birman, Solid State Commun. **13**, 1189 (1973).
[13]R. J. Elliot, Phys. Rev. **124**, 340 (1961).
[14]B. Dayal, Proc. Indian Acad. Sci. **32A**, 304 (1950).
[15]R. Loudon, Proc. R. Soc. London Ser. A **275**, 218 (1963).
[16]J. L. Birman, Phys. Rev. B **9**, 4518 (1974); J. L. Birman and A. K. Ganguly, Phys. Rev. Lett. **17**, 647 (1966); Phys. Rev. **162**, B806 (1967).
[17]M. Cardona and G. Harbeke, Phys. Rev. **137**, 1467 (1965).
[18]D. M. Eagles, J. Phys. Chem. Solids **25**, 1243 (1964).
[19]E. F. Gross, S. A. Bermogorov, and B. S. Razbirin, Fiz. Tverd. Tela (Leningrad) **8**, 1483 (1966) [Sov. Phys. Solid State **8**, 1180 (1966)]; J. Phys. Chem. Solids **27**, 1647 (1966).
[20]B. Segall and G. D. Mahan, Phys. Rev. **171**, 935 (1968).
[21]S. P. S. Porto, P. A. Fleury, and T. C. Damen, Phys. Rev. **154**, 522 (1967).
[22]A. Compaan and H. Z. Cummins, Phys. Rev. Lett. **31**, 41 (1973).
[23]M. Inoue and Y. Toyozawa, J. Phys. Soc. Jpn. **20**, 363 (1965).